SAND--89-0780C

DE89 009334

FINITE CONTROL VOLUME MODELING OF LAMINAR AND TURBULENT FLOW OF AIR IN AN ENCLOSURE

R. E. Hogan, Jr.* and C. F. Kettleborough
Texas A&M University
College Station, TX 77843

Abstract

The finite control volume method (FCVM) was successfully used to calculate both laminar and turbulent buoyancy driven flow of air in a square enclosure for $Ra = 10^3$ to 10^8. For laminar flow, comparisons of the computed solution with both experimental data [15,17,18] and other numerical solutions [20] are in excellent agreement. Comparisons of selected velocities and average Nusselt numbers with a "benchmark" solution presented by deVahl Davis [20] are consistently within 4%. For turbulent flow, the agreement with another numerical solution [13] is generally good, considering the large difference in the number of nodes employed. The agreement with extrapolated experimental correlations for the average Nusselt number was acceptable.

1 Introduction

In 1978, Baliga [1] developed the FCVM using triangular elements for the solution of diffusion-convection and fluid flow/heat transfer problems. In 1979, Hogan and Blackwell [2] independently developed a transient FCVM for diffusion problems. The FCVM combines the advantages of both finite difference methods (FDM) and finite element methods (FEM). It has been used to solve many different fluid flow and heat transfer problems and the computed results compare well with other results.

*Currently employed at Sandia National Laboratories, Albuquerque, NM 87185

In many cases, the FCVM solutions for diffusion problems are up to two orders of magnitude more accurate than those computed by other methods [3,4,5]. For convection-diffusion problems, the "false" or "numerical" diffusion associated with the FCVM is significantly less than with upwind difference FDM. Baliga and Patankar [6] show the FCVM error is less than the FDM using upwind, hybrid, and power law differencing schemes. The use of an elemental coordinate system with a novel exponential differencing scheme based on the local flow conditions [7] reduces this error.

Fluid flow/heat transfer problems have been solved by the FCVM for laminar flows in closed domains. Hogan [8] used the FCVM to solve turbulent flows over both closed and open domains. This paper presents FCVM solutions for both laminar and turbulent buoyant motion of air in a square enclosure for $Ra = 10^3$ to 10^8. The FCVM applicability for buoyancy driven flows with variable fluid properties, in particular, for turbulent flows, is demonstrated.

2 Finite Control Volume Method

Mathematically, the FCVM is a subdomain method, a subclass of the FEM of weighted residuals with the weighting function unity over the "control volume" and zero elsewhere. Physically, it is an application of conservation principles for finite-sized control volumes. A representative convection-diffusion equation for a generalized field variable, ϕ, in flux vector form is

$$\frac{\partial}{\partial t}(\rho\phi) + \nabla \cdot \vec{J} = S_p\phi + S_c \ , \tag{1}$$

where $\vec{J} = \rho\vec{V}\phi - \Gamma_\phi \nabla\phi$. With the proper choice of ϕ, Γ_ϕ, S_p, and S_c, Eq. (1) reduces to conservation of mass, linear momentum, energy, etc. Conservation of ϕ over an arbitrary control volume is

$$\frac{\partial}{\partial t}\int_{CV} \rho\phi \, dV + \int_{CS} \vec{J} \cdot \hat{n} \, dA = \int_{CV} (S_p\phi + S_c) \, dV, \tag{2}$$

where CV and CS represent integration over the control volume and control surfaces, respectively.

As with FEMs, the domain of interest is divided into triangular elements with ϕ nodes at each of the vertices as shown in Fig. 1. For a 2-D problem, integration over the control volume simplifies to an area integral (hashed area), and integration over the control surfaces simplifies to a line integral (dashed lines). Profiles for ρ, S_p, and S_c are assumed constant and Γ_ϕ and the velocities (convective terms) are assumed linear over the element. The velocities are evaluated at the pre-

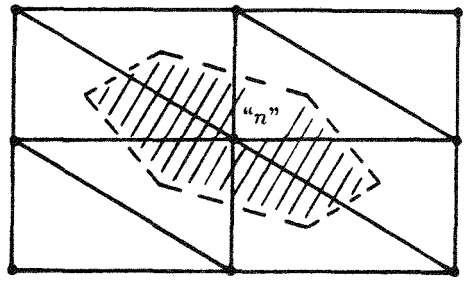

Figure 1: Typical element and control volume configuration

vious iteration. Due to the convective nature of the flow, the ϕ profile is assumed expontential in the streamwise (locally) direction and linear in the cross-stream direction [1]. Each element has contributions to the control volumes about each of its nodes. These contributions are computed on an element-by-element basis and merged into a global matrix similar to the FEM.

3 Mathematical Formulation

For turbulent flow of an incompressible fluid with negligible viscous dissipation and no internal heat generation, the time-averaged equations (indicial notation) for conservation of mass, momentum, and energy in dimensionless form are

$$\frac{\partial \overline{u_i^*}}{\partial x_i^*} = 0 \,, \tag{3}$$

$$\frac{\partial \overline{u_i^*}}{\partial t^*} + \overline{u_j^*}\frac{\partial \overline{u_i^*}}{\partial x_j^*} = \frac{1}{Re}\frac{\partial}{\partial x_j^*}\left(\nu_e^*\frac{\partial \overline{u_i^*}}{\partial x_j^*}\right) - \frac{\partial \overline{P}^*}{\partial x_i^*} - \frac{Gr}{Re^2}\overline{B_i^*} + \frac{1}{Re}\frac{\partial}{\partial x_j^*}\left(\nu_e^*\frac{\partial \overline{u_j^*}}{\partial x_i^*}\right) \,, \tag{4}$$

and

$$\frac{\partial \overline{T}^*}{\partial t^*} + \overline{u_i^*}\frac{\partial \overline{T}^*}{\partial x_i^*} = \frac{1}{Re}\frac{\partial}{\partial x_i^*}\left[\left(\frac{\alpha^*}{Pr} + \frac{\nu_T^*}{\sigma_T}\right)\frac{\partial \overline{T}^*}{\partial x_i^*}\right] \,, \tag{5}$$

where $\nu_e^* = \nu^* + \nu_T^*$ and $\overline{B_i^*} = g_i^*\beta^*\overline{T}^*$ is the buoyancy.

For laminar flow, Eqs. (3-5) are simplified using $\nu_T = 0.0$ and $\nu_e^* = \nu^*$. For turbulent flow, they can be solved if the turbulent viscosity and the turbulent Prandtl number are known. The turbulent heat flux is expressed using the Reynolds analogy between heat and mass transfer [9,10]. For the two-equation turbulence model, the turbulent viscosity [11,9] is $\nu_T^* = C_\mu Rek^{*^2}/\epsilon^*$. After simplification [9,12], the modeled form of the turbulent kinetic energy and the turbulent kinetic

energy dissipation rate equations are

$$\frac{\partial k^*}{\partial t^*} + \overline{u_i^*}\frac{\partial k^*}{\partial x_i^*} = \frac{1}{Re}\frac{\partial}{\partial x_i^*}\left(\frac{\nu_T^*}{\sigma_k}\frac{\partial k^*}{\partial x_i^*}\right) + \frac{1}{Re}G_S^* - \epsilon^* \,, \tag{6}$$

and

$$\frac{\partial \epsilon^*}{\partial t^*} + \overline{u_i^*}\frac{\partial \epsilon^*}{\partial x_i^*} = \frac{1}{Re}\frac{\partial}{\partial x_i^*}\left(\frac{\nu_T^*}{\sigma_\epsilon}\frac{\partial \epsilon^*}{\partial x_i^*}\right) + \frac{C_1}{Re}\frac{\epsilon^*}{k^*}G_S^* - C_2\frac{{\epsilon^*}^2}{k^*} \,, \tag{7}$$

where

$$G_S^* = \nu_T^*\left(\frac{\partial \overline{u_i^*}}{\partial x_j^*} + \frac{\partial \overline{u_j^*}}{\partial x_i^*}\right)\frac{\partial \overline{u_i^*}}{\partial x_j^*} \tag{8}$$

and σ_k and σ_ϵ are the ratios of the turbulent viscosity to the diffusivity of turbulent kinetic energy and turbulent kinetic energy dissipation rate, respectively. Values for the empirical constants [13] are $C_1 = 1.44$, $C_2 = 1.92$, $C_\mu = 0.09$, $\sigma_T = 1.00$, $\sigma_k = 1.00$, and $\sigma_\epsilon = 1.314$.

Boundary conditions are imposed by "jumping" or "bridging" the viscous sublayer, including its influence on the mean flow using the "wall functions." A typical boundary node is near, but not at, the wall. For this discussion, the y^+ coordinate refers to the "wall coordinate," measured normal to and away from the wall and the u velocity refers to the velocity component parallel to the wall.

The momentum boundary conditions are imposed by specifing zero velocity normal to the wall. The velocity gradient (shear stress) parallel to the wall is imposed using the log-law relationship for a turbulent boundary layer. The location of the near-wall nodes must be outside the viscous sublayer or $y^+ \geq 11.5$, where, $y^+ = yu_\tau/\nu = y^* u_\tau^* Re$. For the viscous sublayer, $y^+ < 11.5$, and for the inertial sublayer [9,11], $y^+ \geq 11.5$, the relationships are

$$u_\tau^* = \frac{|u^*|}{y^+} \qquad \text{and} \qquad u_\tau^* = \frac{|u^*|\kappa}{ln[E\ y^+]} \,, \tag{9}$$

respectively, where $\kappa = 0.419$, and $E = 9.793$. For turbulent flow, all near-wall nodes must be in the inertial sublayer, $y^+ \geq 11.5$. The boundary condition for conservation of energy is imposed using the boundary heat flux

$$\dot{q}_w''^* = \rho^*\ u^*\ C_p^*\ Re\ St\ Pr\ (T^* - T_w^*) \,, \tag{10}$$

which is a function of the temperature at the wall and the velocity, velocity gradient, and temperature at the near-wall node. Assuming the turbulence is in local equilibrium near the wall, the boundary conditions for k^* and ϵ^* are $k^* = |\tau_w^*|/\sqrt{C_\mu}$ and $\epsilon^* = |\tau_w^*|^{1.5}/\kappa y^*$, respectively. At the begining of each iteration, these boundary conditions are recalculated and respecified using velocities, velocity gradients, and temperatures from the previous iteration.

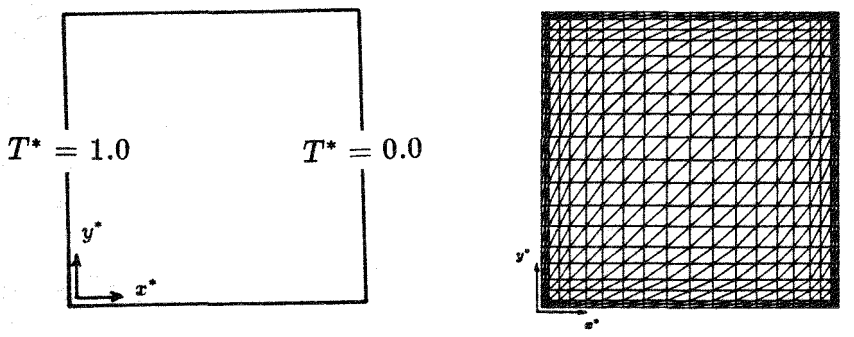

Figure 2: Geometry and Typical Grid for Example Problems

4 Example Problems

A common test problem is the buoyancy driven flow of air in a square enclosure. Figure 2 shows the basic enclosure geometry and a typical grid. A nonuniform grid is used for all solutions. The horizontal walls are assumed to be adiabatic and the vertical are assumed isothermal. The wall at $x^* = 0.005$ is maintained at $T^* = 1.0$ and at $x^* = 0.995$, $T^* = 0.0$. The Rayleigh number is varied from 10^3 to 10^8. The transition to turbulent flow has been observed at approximately $Ra = 10^6$ [15,16], so the flow is assumed turbulent for $Ra > 10^6$.

For laminar flow, 21×21 and 31×31 nonuniform grids are used and for turbulent flow, ($Ra = 10^8$), 31×31 and 41×41 grids. The initial velocities and temperatures are zero. The initial turbulence kinetic energy and turbulence kinetic energy dissipation rate are 1000 and 1, respectively. Relaxation factors for u^*, v^*, T^*, k^*, ϵ^*, and P^* are initially 0.5, 0.5, 0.05, 0.5, 0.5, and 0.6, respectively. They are increased to 0.6, 0.6, 0.4, 0.5, 0.5, and 0.7 as the solution progresses. Since this flow is buoyancy driven, convergence is very sensitive to the temperature relaxation factor during the early iterations.

4.1 Computed Results

Figure 3 shows the vertical velocity profiles along a plane of $y^* = 0.5$. As the Rayleigh number increases the peak velocity increases, its location moves towards the walls, and the size of the low velocity region increases. For $Ra \geq 10^5$, a flow reversal occurs near the interface of the central core and the boundary layer. An analysis of the streamlines [8] show the presence of vorticies at this interface. For turbulent flow, $Ra = 10^8$, the maximum velocities increase approximately an order of magnitude, the boundary layer is thinner, and velocity peaks are closer to the walls.

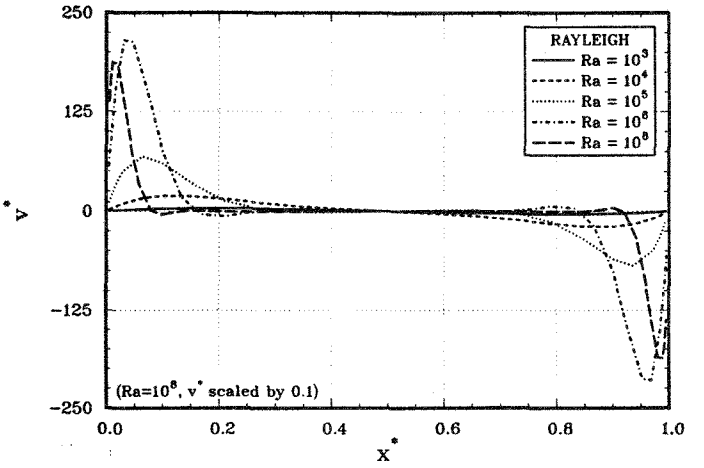

Figure 3: Vertical velocity profiles along the horizontal mid-plane, $y^* = 0.5$, for varying Rayleigh number.

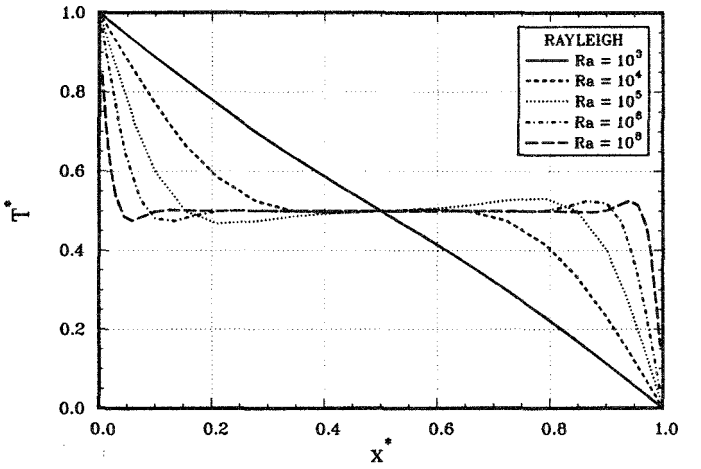

Figure 4: Temperature profiles along the horizontal mid-plane, $y^* = 0.5$, for varying Rayleigh number.

Figure 4 shows the temperature profiles along a horizontal plane, $y^* = 0.5$. For $Ra = 10^3$, the heat transfer is dominated by conduction, the horizontal temperature gradient is negative, and the temperature profile is almost linear. As the Rayleigh number increases, the gradients near both of the walls are increasingly negative, and the size of the isothermal region increases.

4.2 Comparison with Experimental Data

An important engineering parameter is the heat transfer across the enclosure, characterized by the average Nusselt number. Table 1 shows a comparison of the computed Average Nusselt number and experimental data for $Ra = 10^3$ to 10^8 [15,17,18]. Due to the lack of available ex-

Table 1: Comparison of computed Nusselt number and experimental data of Elder [15], Jacob [17], and Eckert and Carlson [18].

	Nu (% difference)			
Ra	FCVM	[15]	[17]	[18]
10^3	1.102	1.413(-22.0)	1.102(0)	1.046(5.4)
10^4	2.212	2.513(-12.0)	1.960(12.9)	2.087(6.0)
10^5	4.387	4.469(-1.8)	3.342(31.3)	4.163(5.4)
10^6	8.503	7.947(7.0)	7.200(18.1)	8.307(2.4)
10^8	31.63	25.13(25.9)	33.419(-5.4)	33.07(-4.4)

perimental data for $Ra = 10^8$, average Nusselt number are compared to extrapolated experimental data. The FCVM solution agrees within 6% of the data of Eckert and Carlson [18]. It agrees reasonably well with the data of Elder [15], but has a different Nu *vs* Ra slope.

4.3 Comparison with Other Numerical Results

A comparison and summary of many of the numerical solutions for this problem is presented by de Vahl Davis [19]. Table 2 compares the FCVM solution with a "benchmark" solution by de Vahl Davis [20] and a donor-cell differencing solution by Markatos and Pericleous [13].

For most cases, these comparisons show the FCVM solution agrees reasonably well with other numerical solutions. For $Ra = 10^3$, there is excellent agreement, with the velocities and the average Nusselt number within a maximum of -1.4% difference (with respect to the "benchmark" solution [20]). For $Ra = 10^4$, there is good agreement, with a -2.2% difference in v_{max}, and for $Ra = 10^5$, the largest percent difference is 3.1% in the velocity u^*_{max}. For $Ra = 10^6$, the horizontal and vertical velocities also agree within 2.8% and -1.9%, respectively. The average Nusselt number is within -3.4%. For $Ra = 10^8$, the percent difference in v^*_{max} is 3.0%, and in the average Nusselt number, only -1.3%. Although neither of these solutions is the absolute "correct" solution, the agreement in these two variables is acceptable, considering the FCVM solution only used 1681 nodes, compared to 7200.

5 Concluding Remarks

The FCVM was successfully used to calculate both laminar and turbulent buoyancy driven flow of air in a square enclosure for $Ra = 10^3$ to

Table 2: Comparison of FCVM Solution with Numerical Solution of de Vahl Davis [20] and Markatios & Pericleous [13]

Ra	Ref.	grid	$u^*_{max}@(0.5, y^*)$	$v^*_{max}@(x^*, 0.5)$	$\overline{Nu}$
10^3	[20]	41×41	3.649@0.813	3.697@0.178	1.118
	FCVM	21×21	3.618@0.791	3.644@0.154	1.102
	[13]	30×30	3.544@0.832	3.593@0.168	1.108
10^4	[20]	41×41	16.18@0.823	19.62@0.119	2.243
	FCVM	21×21	16.14@0.846	19.18@0.100	2.212
	[13]	30×30	16.18@0.832	19.44@0.113	2.201
10^5	[20]	81×81	34.73@0.855	68.59@0.066	4.519
	FCVM	21×21	35.81@0.846	68.61@0.064	4.387
	[13]	40×40	35.73@0.857	69.08@0.067	4.430
10^6	[20]	81×81	64.63@0.850	219.4@0.0379	8.799
	FCVM	31×31	66.42@0.866	215.2@0.0318	8.503
	[13]	40×40	68.81@0.872	221.8@0.0375	8.754
10^8	FCVM	31×31	382.0@0.952	1924.0@0.0158	31.724
	FCVM	41×41	339.3@0.941	1867.0@0.0111	31.625
	[13]	60×120	514.3@0.941	1812.0@0.0135	32.045

10^8. The computed results include both the vertical velocity and the temperature across the horizontal mid-plane and the average Nusselt number. Additional details and more results, including isotherms and streamlines, are presented in [8].

For both laminar and turbulent flow, the computed average Nusselt number agree well with both experimental data and other numerical solutions. Selected velocities and the average Nusselt number are within 4% of the other numerical solutions. Generally, comparisons show acceptable agreement with both experimental data and numerical solutions that use considerably more nodes. This suggests the reduction in "false" diffusion associated with the FCVM is significant, resulting in comparable accuracy with fewer nodes.

Nomenclature

C_1, C_2, C_μ	turbulence model constants
C_f	coefficient of friction, $C_f \equiv \frac{\tau^*_w}{\lvert u^* \rvert^2}$
C^*_p	specific heat, $C^*_p \equiv \frac{C_p}{C_{p_\circ}}$
g_i	gravity vector
Gr	Grashoff number, $Gr \equiv \frac{g\beta_\circ \rho^2_\circ h^3_\circ (T_h - T_c)}{\mu^2_\circ}$
h	length of cavity side

k^*	turbulent kinetic energy, $k^* \equiv \frac{k}{u_\circ^2}$
$\hat{n}$	outward normal unit vector
Nu	Nusselt number, $Nu \equiv \frac{q''_w h_\circ}{k_\circ(T_h - T_c)}$
P^*	pressure, $P^* \equiv \frac{P+\rho_\circ g y - P_\circ}{\rho u_\circ^2}$
Pr	Prandtl number, $Pr \equiv \frac{\mu_\circ C_{p\circ}}{K_\circ}$
$\dot{q}''^*_w$	heat flux, $\dot{q}''^*_w \equiv \frac{q''_w h_\circ}{k_\circ(T_h - T_c)}$
Ra	Rayleigh number, $Ra \equiv GrPr$
Re	Reynolds number, $Re \equiv \frac{\rho_\circ u_\circ h_\circ}{\mu_\circ}$
S_c	constant volumetric generation
S_p	phi dependent volumetric generation
St	Stanton number, $St \equiv C_f Pr^{-2/3}$
t^*	time, $t^* \equiv \frac{t u_\circ}{h_\circ}$
T^*	temperature, $T^* \equiv \frac{(T-T_c)}{(T_h - T_c)}$
u_i^*	velocities, $u_i^* \equiv u_i / u_\circ$
u_τ^*	shear velocity, $u_\tau^* \equiv \sqrt{\tau_w^*}$
x_i^*	coordinates, $x_i^* \equiv \frac{x_i}{h_\circ}$
Greek	
α	thermal diffusivity
β	coefficient of thermal expansion, $\beta \equiv 1/T$
ϵ^*	turbulent kinetic energy dissipation rate, $\epsilon^* \equiv \frac{\epsilon h_\circ}{u_\circ^3}$
Γ_ϕ	generalized diffusion coefficient
K^*	thermal conductivity, $K^* \equiv \frac{K}{K_\circ}$
μ^*	dynamic viscosity, $\mu^* \equiv \frac{\mu}{\mu_\circ}$
ν^*	kinematic viscostiy, $\nu^* \equiv \frac{\nu}{\nu_\circ}$
ϕ	generalized field variable
ρ^*	fluid density, $\rho^* \equiv \frac{\rho}{\rho_\circ}$
σ_T	turbulent Prandtl number
τ_w^*	wall shear stress, $\tau_w^* \equiv \tau_w / \rho u_\circ^2$
Subscript	
i, j	indicial notation
c	cold wall
e	effective
h	hot wall
T	turbulent
$\circ$	reference variable
Superscript	
$*$	dimensionless quantity

References

[1] B. R. Baliga, "A Control-Volume Based Finite Element Method for Convective Heat and Mass Transfer," Ph.D. thesis, University of Minnesota, Minneapolis, Minnesota, 1978.

[2] R. E. Hogan, Jr. and B. F. Blackwell, "Comparison of Numerical Model with ASHRAE Design Procedure for Warm Water Concrete F oor Heating Panels," *ASHRAE Transactions*, vol. 92, pt. 1, 1986.

[3] S. Ramadhyani and S. V. Patankar, "Solution of the Poisson Equation: Comparison of the Galerkin and Control-Volume Methods," *International Journal for Numerical Methods in Engineering*, 15, 1395-1418, 1980.

[4] G. E. Schneider and M. Zedan, "Control Volume Based Finite Element Formulation of the Heat Conduction Equation," AIAA/ASME 3^{rd} Joint Thermophysics, Fluids, Plasma and Heat Transfer Conference, St. Louis, Missouri, June 7-11, 1982.

[5] M. J. Raw, G. E. Schneider and V. Hassani, "Development and Evaluation of Nine-Noded Quadratic Control Volume Based Finite Element for Heat Conduction Modelling," AIAA 22^{nd} Aerospace Sciences Meeting, Reno, Nevada, January 9-12, 1984.

[6] B. R. Baliga and S. V. Patankar, "A New Finite-Element Formulation for Convection-Diffusion Problems," *Numerical Heat Transfer*, 3, 393-409, 1980.

[7] S. V. Patankar and B. R. Baliga, "A New Finite-Difference Scheme for Parabolic Differential Equations," *Numerical Heat Transfer*, 1, 27-37, 1978.

[8] R. E. Hogan, Jr., "Finite Control Volume Modeling of the Turbulent Motion of Air in an Enclosure," Ph.D. thesis, Texas A&M University, College Station, Texas, 1987.

[9] W. Rodi, *Turbulence Models and Their Application in Hydraulics*, Book Publication of the International Association for Hydraulic Research, Delft, the Netherlands, 1980.

[10] D. B. Spalding, *Turbulence Models for Heat Transfer*, Research Report HTS-78-2, Heat Transfer Section, Imperial College of Science and Technology, London, U K., 1978.

[11] B. E. Launder and D. B. Spalding, "The Numerical Computation of Turbulent Flows," *Computer Methods in Applied Mechanics and Engineering*, 3, 269-289, 1974.

[12] H. Tennekes and J. L. Lumley, *A First Course in Turbulence*, MIT Press, Cambridge, Massachusetts, 1972.

[13] N. C. Markatos and K. A. Pericleous, "Laminar and Turbulent Natural Convection in an Enclosed Cavity," *International Journal of Heat and Mass Transfer*, 27, no. 5, 755-772, 1984.

[14] J. L. Lumley, "Turbulence Modeling," *Journal of Applied Mechanics*, 50, 1097-1103, 1980.

[15] J. W. Elder, "Turbulent Free Convection in a Vertical Slot," *Journal of Fluid Mechanics*, 23, 99-111, 1965.

[16] G. H. Cowan, P. C. Lovegrove and G. L. Quarini, "Turbulent Natural Convection Heat Transfer in Vertical Single Water-Filled Cavities," *Proceedings of* 7^{th} *International Heat Transfer Conference*, 2, 195-201, 1982.

[17] M. Jacob, *Heat Transfer*, Wiley, pg. 538, New York, New York, 1957.

[18] E. R. G. Eckert and W. O. Carlson, "Natural Convection in an Air Layer Enclosed Between Two Vertical Plates with Different Temperatures," *International Journal of Heat and Mass Transfer*, 2, 106-120, 1961.

[19] G. de Vahl Davis and I. P. Jones, "Natural Convection in a Square Cavity: A Comparison Exercise," *Numerical Methods in Thermal Problems*, eds. R. W. Lewis, K. Morgan and B. A. Schrefler, Swansea, U. K., Pineridge Press, 1981.

[20] G. de Vahl Davis, "Natural Convection of Air in a Square Cavity: A Bench Mark Numerical Solution," *International Journal for Numerical Methods in Fluids*, 3, 249-264, 1983.